Energy Engineering

Tech Science Press

http://doi.org/10.32604/ee.2026.082598

ARTICLE

Techno-Economic and Life Cycle Assessment for a Hydrogen Production System Using Renewable Energy

Yutong Lei*, Zhongchao Yang, Xingyu Liu, Mingtao Tang and Mingchen Yao

Changzhou Changgong Electric Power Design Institute Co., Ltd., Changzhou, China
*Corresponding Author: Yutong Lei. Email: leiyt@js.sgcc.com.cn

Received: 18 March 2026; Accepted: 17 September 2026; Published: 12 November 2026

ABSTRACT: Distributed hydrogen production has garnered significant attention due to its potential to reduce transportation costs and utilize local renewable energy sources. This study develops a comprehensive life cycle assessment (LCA) and techno-economic analysis framework for distributed hydrogen production based on a 100 MW alkaline water electrolysis system modeled in Aspen Plus. The process simulation provides detailed mass and energy balances to quantify the system's performance across three key dimensions: environmental, economic, and energy. Environmentally, when powered by photovoltaic electricity, the system achieves a total life cycle carbon footprint of 1.94 kg CO_2eq/kg H_2, with approximately 91% of emissions originating from the electrolyzer's power consumption. Economically, the levelized cost of hydrogen (LCOH) is calculated at 25.403 CNY/kg, placing the system competitively within current green hydrogen estimates, though it remains above traditional fossil-based routes. Energetically, the system exhibits an overall energy efficiency of 56.57% and an exergy efficiency of 55.61%, revealing that system irreversibility (exergy destruction) is predominantly concentrated within the electrolyzer unit. Sensitivity analysis indicates that annual operating hours (capacity factor) and renewable power carbon intensity (electricity prices) are the most critical drivers for economic viability. Therefore, securing low-carbon, low-price renewable electricity and extending operational hours are essential to enhancing the competitiveness of distributed hydrogen production.

KEYWORDS: Distributed hydrogen production; life cycle assessment; techno-economic analysis; exergy analysis

1 Introduction

Amid global efforts to address climate change and advance the energy transition, hydrogen energy has emerged as a strategically significant clean secondary energy carrier. Driven by national carbon neutrality targets, supportive policies are actively fostering hydrogen-related R&D, hydrogen production capacity, and the development of refueling infrastructure, thereby accelerating the shift from demonstration projects to large-scale adoption. In recent years, renewable energy-powered water electrolysis has developed rapidly, with many countries setting hydrogen deployment targets beyond the transportation sector-including industry, buildings, and power generation-and demonstrating active planning and pilot initiatives [1]. Distributed hydrogen production has gained increasing attention as an innovative approach to hydrogen generation. By leveraging the geographical advantages of renewable energy sources such as wind and solar, distributed systems can facilitate the local utilization of renewable electricity and reduce the need for long-distance energy transmission. These systems can also improve the flexibility of hydrogen production in response to regional renewable resource availability, thereby further advancing regional low-carbon economic development [2].

Copyright © 2027 The Authors. Published by Tech Science Press. This work is licensed under a Creative Commons Attribution 4.0 International License, which permits unrestricted use, distribution, and reproduction in any medium, provided the original work is properly cited.

Currently, the main distributed hydrogen production technologies include alkaline water electrolysis (AWE), proton exchange membrane electrolysis (PEM), and solid oxide electrolysis (SOEC) [3]. In recent years, AWE and PEM have become the two dominant technologies in green hydrogen production. AWE, as the primary technology in terms of installed capacity, accounts for approximately 60% of global electrolyzer capacity and is widely used in industrial decarbonization sectors such as steel and chemicals-exemplified by projects like Sweden's HYBRIT green hydrogen-based steelmaking initiative [4] and Saudi Arabia's large-scale green ammonia plants. In transportation and energy systems, hydrogen produced via AWE is already being used in fuel cell trains [5] and integrated into "power-to-gas" projects for wind energy storage and grid balancing [6]. PEM technology is undergoing rapid commercialization, led by companies such as Norway's Nel and Canada's Cummins, which have introduced megawatt-scale systems with hydrogen production capacities of 4000–5000 Nm^3/h and operating pressures of up to 30 bar. These systems exhibit energy consumptions around 4.3–4.5 kWh/Nm^3 H_2, with advantages including fast response and high-purity output, making them suitable for integration with intermittent renewable energy sources. PEM's market share continues to expand globally [7]. In contrast, SOEC technology remains less mature, largely confined to laboratory and demonstration stages, with a technology readiness level (TRL) of around 5 and typical single-stack capacities at the kW scale. Although SOEC offers significantly higher efficiency compared to AWE and PEM, it faces challenges such as long start-up and shutdown times, material corrosion at high temperatures, and rapid performance degradation (e.g., several percentage points over 1000 h of operation) [8,9]. Internationally, the Idaho National Laboratory in the United States and Germany's Sunfire have developed 15 kW and 720 kW stacks, respectively, with the latter aiming for hundred-ton-scale green hydrogen production by the end of 2022. In China, institutions such as the Dalian Institute of Chemical Physics (Chinese Academy of Sciences) and Tsinghua University have conducted preliminary research on kW-scale reversible solid oxide cells, though overall progress still lags behind international advanced levels [8].

Regarding centralized, ultra-large-scale renewable hydrogen production pathways, existing studies have conducted in-depth explorations of their technical-economic feasibility and future cost trends through integrated system modeling. These studies typically use the levelized cost of hydrogen (LCOH) as a core evaluation metric, with calculation methods encompassing capital investment, operational costs, and discounted cash flows. Results indicate that in such projects, electricity consumption, electricity price, and investment in system components are among the most critical factors influencing hydrogen production costs [10]. In terms of carbon footprint assessment for water electrolysis hydrogen production systems, existing research widely employs process-based life cycle assessment (LCA) methodology. This approach enables the environmental impacts of hydrogen production to be systematically quantified by considering the life-cycle inventory, energy consumption, material inputs, and electricity sources associated with electrolysis systems [11]. For the economic analysis of water electrolysis hydrogen production, existing studies have identified that costs are primarily driven by electrolyzer investment and electricity consumption, with alkaline electrolyzers benefiting from relatively low investment requirements. Techno-economic assessments further indicate that reducing electrolyzer costs and electricity prices is essential for improving the competitiveness of alkaline water electrolysis, while the electricity source and price also have significant effects on the overall economic performance [12].

Life Cycle Assessment (LCA) provides a comprehensive methodological framework for quantitatively characterizing the environmental burdens of energy systems from "cradle to grave," covering stages such as raw material extraction, plant construction, operation, decommissioning, and related upstream and downstream processes. When coupled with rigorous process simulation, LCA can accurately depict material

and energy flows, yield more reliable environmental inventories and enable robust sensitivity analyses. Aspen Plus is one of the most widely used process simulation platforms in chemical and energy systems, offering comprehensive thermodynamic models, flexible process modeling capabilities, and well-developed mass and energy balance tools. Integrating Aspen Plus with LCA provides a powerful approach for evaluating distributed hydrogen production technologies under various scenarios and boundary conditions.

Despite rapid advancements in hydrogen-related research in recent years, existing LCA studies have predominantly focused on centralized, large-scale hydrogen production facilities or single pathways (e.g., steam methane reforming or grid-powered water electrolysis), with relatively limited attention given to distributed hydrogen production systems. Alkaline water electrolysis, one of the most mature and widely adopted green hydrogen production methods, represents a key direction for future distributed hydrogen development. Therefore, this study employs an Aspen Plus-based process model as the core tool for inventory generation to conduct a comprehensive life cycle assessment of renewable-powered alkaline water electrolysis hydrogen production, evaluating its performance across three dimensions: carbon footprint, economic viability, and energy efficiency.

Despite the established body of literature on hydrogen energy systems, existing LCA and TEA evaluations have predominantly focused on centralized, large-scale hydrogen production facilities or generic, single-pathway supply chains. The distinct novelty and contribution of this study lie in establishing a comprehensive, high-resolution evaluation framework tailored specifically for distributed alkaline water electrolysis (AWE) systems dynamically integrated with diverse localized renewable energy configurations. Going beyond standard high-level economic inventories or decoupled empirical assumptions, this research leverages steady-state Aspen Plus process simulations to rigorously map internal thermodynamic behaviors, explicitly quantifying the exergy destruction distributions across specific operational sub-units (including cooling, compression, and purification stages). This integrated approach successfully bridges the analytical gap between micro-level process thermodynamics and macro-level environmental and levelized cost profiles, offering granular engineering insights for the strategic deployment and market integration of distributed green hydrogen infrastructure.

2 Distributed Hydrogen Production

The typical technical route of a distributed hydrogen production system is shown in Fig. 1. Its core process covers three main links: power supply from renewable energy, hydrogen production through water electrolysis, and hydrogen storage and diversified utilization. The system's electricity can be sourced from clean energy such as solar and wind power or the power grid; the electricity drives the water electrolysis system to produce hydrogen; the produced hydrogen, after storage, can be directly used for power generation through fuel cells or as raw material for the synthesis of ammonia, methanol and other chemicals. The research object of this paper is the key production unit in this technical route—the alkaline water electrolysis hydrogen production system.

Modeling and process simulation were conducted for a 100 MW electrolyzer, with an integrated energy production system established. The alkaline water electrolysis (AWE) system consists of an anode, a cathode, a power supply, and an electrolyte. A direct current (DC) is applied to maintain electrical balance. Electrons flow from the negative terminal of the DC power source to the cathode of the electrolyzer, where they combine with hydrogen ions (protons) to form hydrogen gas. To maintain charge balance, hydroxide ions (anions) migrate through the electrolyte to the anode. At the anode, hydroxide ions release electrons, which return to the positive terminal of the DC power supply. To enhance the conductivity of the solution, an electrolyte composed of highly mobile ions is typically used. Potassium hydroxide (KOH) is the most

common electrolyte in water electrolysis because it avoids the corrosion issues associated with acidic electrolytes. Nickel is a widely adopted electrode material due to its high activity, availability, and low cost. A diaphragm is employed to separate the gases, allowing gas collectors to capture the hydrogen and oxygen generated at the cathode and anode, respectively.

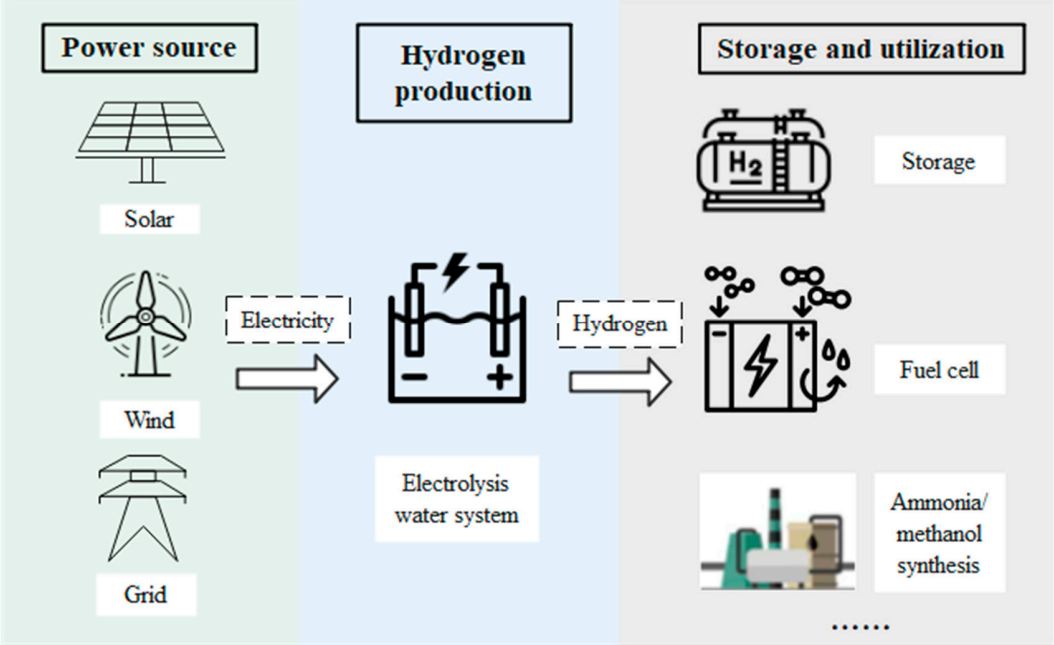


Figure 1: Schematic diagram of a distributed hydrogen production system.

The reactions in an alkaline electrolyzer are expressed by Eqs. (1)–(3):
Anode:

$$2OH^- \rightarrow 0.5O_2 + H_2O + 2e^- \tag{1}$$

Cathode:

$$2H_2O + 2e^- \rightarrow H_2 + 2OH^- \tag{2}$$

Overall Reaction:

$$H_2O \rightarrow H_2 + 0.5O_2 \tag{3}$$

The standard molar enthalpy change, standard molar entropy change, and standard molar Gibbs free energy change of this reaction are as follows:

$$\Delta_r H_m^\theta = 285.83\ \text{kJ} \cdot \text{mol}^{-1} \tag{4}$$

$$\Delta_r S_m^\theta = 163.343\ \text{J} \cdot \text{mol}^{-1} \cdot \text{K}^{-1} \tag{5}$$

$$\Delta_r G_m^\theta = \Delta_r H_m^\theta - T \cdot \Delta_r S_m^\theta = 237.13\ \text{kJ} \cdot \text{mol}^{-1} \tag{6}$$

The actual single-cell voltage can be expressed as the sum of the reversible voltage, activation overpotential, ohmic overpotential, and concentration overpotential. The electrochemical model is as follows:

$$V_{cell} = V_{rev} + (\eta_{cat} + \eta_{an} + \eta_{ohm} + \eta_{conc}) \tag{7}$$

where V_{cell} denotes the actual operating voltage of a single cell (V); V_{rev} is the reversible thermodynamic decomposition voltage (V); η_{cat} represents the activation overpotential of the cathodic hydrogen evolution reaction (V); η_{an} represents the activation overpotential of the anodic oxygen evolution reaction (V); η_{ohm} denotes the total ohmic overpotential of the system (V); and η_{conc} denotes the concentration overpotential (V).

The polarization curve can be determined using a semi-empirical model, which includes additional parameters and empirical correlations with temperature, pressure, and current density:

$$V_{\text{cell}} = V_{\text{rev}} + [(r_1 + d_1) + r_2 \cdot T + d_2 \cdot p]i + s \cdot \log\left[\left(t_1 + \frac{t_2}{T} + \frac{t_3}{T^2}\right)i + 1\right] \tag{8}$$

where i represents the operating current density of the electrolyzer ($A{\cdot}cm^{-2}$); T is the thermodynamic operating temperature of the electrolyzer (K); p is the operating pressure of the electrolyzer (bar); r_1 is the baseline empirical coefficient for ohmic losses from electrodes and electrolyte ($\Omega{\cdot}cm^2$); d_1 is the baseline empirical coefficient for diaphragm resistance ($\Omega{\cdot}cm^2$); r_2 is the temperature correction coefficient for ohmic losses ($\Omega{\cdot}cm^2{\cdot}K^{-1}$); d_2 is the pressure correction coefficient for ohmic losses ($\Omega{\cdot}cm^2{\cdot}bar^{-1}$); s is the Tafel empirical coefficient for activation overpotential (V); and t_1, t_2 and t_3 are temperature correction coefficients for activation losses, with t_1 as the baseline term, t_2 as the first-order temperature correction term, and t_3 as the second-order temperature correction term.

The hydrogen and oxygen production rates depend on the electrochemical behavior of the cell and can be calculated using Faraday's efficiency:

$$n_{\text{H}_2,\text{prod}} = n_F \cdot \frac{I}{z \cdot F} \cdot N \tag{9}$$

$$n_{\text{O}_2,\text{an}} = n_{\text{O}_2,\text{prod}} = \frac{1}{2} n_{\text{H}_2,\text{prod}} \tag{10}$$

where $n_{\text{H}_2,\text{prod}}$ denotes the total hydrogen production rate of the stack ($mol{\cdot}s^{-1}$); η_F is the Faraday efficiency (dimensionless); I represents the current of a single cell (A); z is the number of electrons transferred per reaction; F is the Faraday constant, equal to 96,485 ($C{\cdot}mol^{-1}$); N is the number of single cells in the stack (dimensionless). and $n_{\text{O}_2,\text{prod}}$ denotes the total oxygen production rate of the stack ($mol{\cdot}s^{-1}$).

Faraday's efficiency can also be expressed as an empirical correlation with four parameters at a given temperature:

$$\eta_F = \left(\frac{i^2}{f_{11} + f_{12} \cdot T + i^2}\right) \cdot (f_{21} + f_{22} \cdot T) \tag{11}$$

where f_{11} and f_{12} are the baseline and temperature correction empirical coefficients for the denominator term of Faraday efficiency (dimensionless); and f_{21} and f_{22} are the baseline and temperature correction empirical coefficients for the correction term of Faraday efficiency (dimensionless).

The coefficients for the empirical correlation can be found in the literature. The power consumption of the AWE stack is:

$$W_{\text{stack}} = V_{\text{stack}} I = V_{\text{cell}} N t A_{\text{cell}} \tag{12}$$

where W_{stack} denotes the total input power of the electrolyzer stack (W); V_{stack} is the total operating voltage of the stack (V); and A_{cell} represents the effective reaction area of a single cell (cm^2). Each electrolyzer stack consists of 380 cells electrically connected in series. Therefore, the stack voltage is the sum of the individual cell voltages, whereas the same current passes through all cells within a stack. At the system level, the 20 identical stacks are connected in parallel. Consequently, all stacks operate at the same voltage, while the total system current is the sum of the currents passing through the individual stacks.

The energy balance equation for the AWE stack is as follows:

$$Q_{\text{gen}} = i A_{\text{cell}} (V_{\text{cell}} - V_{\text{th}}) N \tag{13}$$

where V_{th} is the thermoneutral voltage, taken as 1.48 V.

The mathematical model of the alkaline electrolyzer presented in this paper describes the polarization curve characteristics of the electrolyzer. The model is based on the following assumptions:

(1) The current efficiency is 100%, neglecting leakage currents and side reactions during the electrolysis process.
(2) Each electrolysis cell in the alkaline electrolyzer has identical electrochemical characteristics, meaning that the current and voltage values for each cell remain consistent.
(3) The temperature and pressure within the electrolyzer are uniformly distributed, i.e., the steady-state average temperature and pressure across all cells are considered constant.
(4) Since hydrogen and oxygen are not easily liquefied under operating conditions, they are treated as ideal gases throughout the electrolysis process.
(5) In addition, since the present study is based on steady-state process simulation using Aspen Plus, the system was assumed to operate under stable operating conditions, and thus dynamic load behavior, partial-load operation, and the influence of fluctuating renewable electricity input on system operation were not further considered. In practical industrial applications, renewable electricity sources such as wind and photovoltaic power exhibit significant intermittency, which may lead to non-full-load operation of electrolyzers and further affect system efficiency and economic performance. To address this limitation, capacity factor was introduced in the techno-economic assessment and sensitivity analysis as a macroscopic proxy variable to characterize the impact of system utilization variations caused by intermittent renewable electricity on the overall economic performance.

The modeling of the renewable energy-based hydrogen production system is illustrated in Fig. 2: Alkaline Water Electrolysis Hydrogen Production System. The system utilizes wind and photovoltaic power as electrical inputs and primarily consists of pumps, alkaline electrolyzers, gas-liquid separators, heat exchangers, dryers, and other components. The supplementary alkali solution is mixed with the recirculated alkali solution, then pressurized and cooled before undergoing electrochemical reactions in the alkaline electrolyzer. The anode and cathode products undergo gas-liquid separation and cooling, followed by drying in dryers. The dried hydrogen and oxygen can be directly sold as products. Key parameters of the electrolyzer are summarized in Table 1.

While these steady-state conditions establish a robust baseline for core mass and energy balances, they inherently introduce potential uncertainties regarding real-world industrial deployment. For instance, the system model simplistically sets the nominal current efficiency at 100%. In practical industrial applications, however, the Faraday efficiency typically fluctuates between 96% and 99% due to localized leakage currents,

gas permeation, and secondary chemical side-reactions [13]. These operational deviations can cause slight variances in absolute quantitative outcomes under transient inputs.

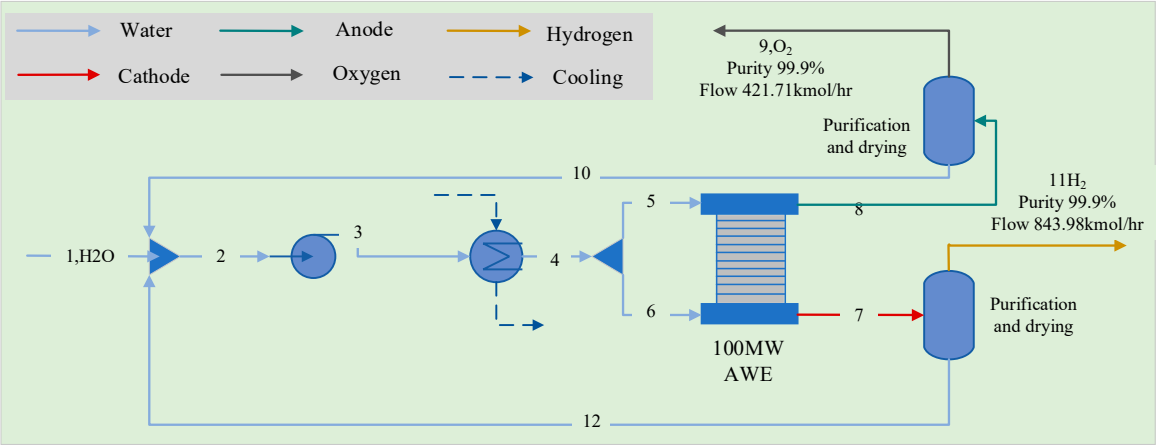


Figure 2: Model of alkaline water electrolysis (AWE) hydrogen production system.

Table 1: Key parameters of alkaline electrolyzer.

Parameter	Value	Unit
Number of Electrolyzer Stacks	20	
Number of Cells per Stack	380	
Operating Pressure	15.8	Bar
Operating Temperature	348	K
Faradaic Efficiency	1	
Cell Efficiency	0.67	
Total DC Input Power of Electrolyzer System	100	MW
Total Operating Current of 20 Parallel Stacks	119,054	A
Operating Current per Stack	5952.7	A
Operating Voltage per Stack	839.953	V

3 Methods

This study provides a comprehensive assessment of the entire renewable energy-powered water electrolysis-to-hydrogen process. The aim is to analyze the environmental impact, economic feasibility, and energy efficiency of the alkaline water electrolysis hydrogen production system, offering a scientific basis for future technological optimization and policy development.

3.1 Life Cycle Assessment

Life Cycle Assessment (LCA) is a systematic methodology used to evaluate the environmental impacts, resource consumption, and potential economic benefits of a product or system across its entire life cycle, from raw material extraction, production, and use to end-of-life treatment. LCA typically comprises four main stages: goal and scope definition, life cycle inventory analysis, life cycle impact assessment, and interpretation of results.

Within the context of the “dual carbon” goals, the significant environmental impact of the greenhouse effect has garnered widespread attention. Life Cycle Assessment (LCA) has become a widely adopted tool for quantifying greenhouse gas (GHG) emissions. In 2007, the Carbon Trust, based on LCA theory, defined carbon footprint as a methodology for estimating the total GHG emissions expressed in carbon dioxide

equivalents (CO_2e) throughout a product's life cycle. This definition expanded the scope of carbon footprint from calculating only CO_2 emissions to encompassing all GHG emissions [14].

In 2013, the International Organization for Standardization (ISO) defined carbon footprint as the total amount of greenhouse gases emitted directly and indirectly across all stages of a product's life cycle, including raw material acquisition, manufacturing, transportation, sale, use, and end-of-life treatment. This definition further refined and improved upon the Carbon Trust's version. The spatiotemporal scope of carbon footprint encompasses the entire product life cycle and includes the calculation of indirect GHG emissions. The definition of carbon footprint has since matured and become more standardized, with the life cycle perspective now established as a key characteristic of its assessment. As a result, the concept of carbon footprint based on LCA has gained increasing acceptance among scholars and has been widely applied to quantify the carbon reduction benefits of large-scale energy production units [15].

This paper uses carbon footprint to assess the global warming potential (GWP) of various greenhouse gases, serving as an index that represents the contribution of a substance to the greenhouse effect. The carbon footprint uses CO_2 as the reference gas. Based on the global warming potential of CO_2 emissions over a 100-year timeframe, other greenhouse gases are converted into an equivalent mass of CO_2 that would produce the same greenhouse effect. These relative values are referred to as CO_2 equivalent factors for greenhouse gases. This study employs the CO_2 emission factor database from US-Title40-Part98 to calculate carbon emissions and CO_2 equivalents for process energy consumption. The calculation formula for the carbon footprint is given by Eq. (14):

$$C_{\mathrm{GWP}} = \sum_i \beta_i \times M_{\mathrm{GHG},i} \tag{14}$$

where β_i represents the CO_2 equivalent factor of greenhouse gas i in kg CO_2eq/kg, and $M_{\mathrm{GHG},i}$ denotes the emission amount of greenhouse gas i in kg. Taking green hydrogen production as an example, its carbon emission equivalent during the production process mainly consists of direct carbon emissions (C_{dir}) and indirect carbon emissions (C_{indir}). Direct carbon emissions primarily refer to greenhouse gas emissions resulting from chemical reactions and similar processes during production. Indirect carbon emissions include emissions caused by energy production, material consumption, waste treatment, and other related activities. The calculation formula is given by Eq. (15):

$$C = C_{\mathrm{dir}} + C_{\mathrm{indir}} = C_{\mathrm{dir}} + C_e + C_m + C_w \tag{15}$$

where C_e represents the carbon footprint generated by electricity consumption during the production process; C_m denotes the carbon footprint resulting from the consumption of raw materials, auxiliary materials, primary and secondary energy sources during production; and C_w indicates the carbon footprint arising from the treatment of waste gases, solid waste, wastewater, waste sand, and other waste materials generated during production. This study assumes that the electricity consumed in the green hydrogen production process is derived from renewable energy sources, while utility electricity is sourced from natural gas.

The calculation of the carbon footprint for secondary energy in C_m is expressed by Eq. (16):

$$C_{m,2} = m_{\mathrm{gas}} \times \mathrm{HHV} \times \beta_{\mathrm{gas}} \times \frac{f_a}{f_e} \tag{16}$$

where m_{gas} represents the converted consumption of secondary energy, HHV denotes the higher heating value of the converted energy, β_{gas} is the carbon emission equivalent factor per unit heating value of the converted energy in kg CO_2eq/kJ, f_a is the CO_2 emission adjustment factor, and f_e represents the CO_2 energy efficiency factor. The values of f_a and f_e are based on the default settings in Aspen software. The CO_2 emission adjustment factor is set to 1, and the CO_2 energy efficiency factor for electricity is 0.58.

3.2 Techno-Economic Assessment

Techno-economic evaluation is a critical step in the decision-making process for water electrolysis hydrogen production projects. The economic analysis of the electrolysis hydrogen production system allows for a quantitative assessment of its economic feasibility and cost competitiveness. In the following sections, computational models will be developed separately for the system's capital costs and operating costs.

To ensure that the techno-economic conclusions are robust and applicable to practical deployment scenarios, the economic evaluation framework in this study is strictly and systematically integrated with the engineering design parameters derived from the process simulation. Instead of relying on static or decoupled empirical inventory values, high-resolution engineering outputs generated from the steady-state Aspen Plus simulation-specifically including the precise mass and energy balances, hourly cooling water consumption, and cumulative auxiliary power requirements of delivery pumps and compressors-are directly routed as dynamic feedforward inputs into the economic model. This rigorous parameter coupling ensures that the operational cost (OPEX) calculations, utility expenses, and sizing scaled factors for equipment procurement are fundamentally rooted in thermodynamic rigor, thereby eliminating unlinked assumptions and reflecting realistic engineering-economic operational boundaries.

3.2.1 Capital Cost

This study evaluates the overall economic performance of the system by calculating the levelized cost of the target product (LCOP) and the net present value (NPV). The levelized cost of hydrogen (LCOH) is calculated as follows:

$$\text{LCOP} = \frac{TCI - \frac{R_s}{(1+r)^N} + \sum_{n=1}^{20} \frac{OPEX}{(1+r)^n}}{\sum_{n=1}^{20} \frac{P}{(1+r)^n}} \tag{17}$$

where TCI represents the Total Capital Investment, OPEX denotes the annual Operating Expenses of the project, and R_s stands for the salvage value, which in this study is assumed to be 10% of TCI. The discount rate r, reflecting the time value of money, is set at 8%. P indicates the annual production of the target product, N is the project lifespan, set at 20 years, and n represents the specific year within the calculation period. The Net Present Value (NPV) is calculated using the following equation:

$$\text{NPV} = \sum_{g=0}^{G^{\text{th year}}} \frac{CF_g}{(1+\text{ROR})^g} \tag{18}$$

where NPV is the net present value in year G; g is the year index; CF_g is the cash flow in year g; and ROR is the internal rate of return.

In practical industrial operation, the core components of alkaline electrolyzers, including electrodes, diaphragms, and sealing structures, gradually experience performance degradation during long-term

operation, which may result in increased electrolyzer voltage, higher electricity consumption, and reduced system efficiency. Previous studies have reported that the lifetime of industrial alkaline electrolyzer stacks can typically reach 8000–10,000 operating hours [16]; however, periodic maintenance and mid-life stack replacement are still required during the project lifecycle.

Therefore, to improve the engineering realism of the techno-economic assessment, the present study incorporates electrolyzer lifetime considerations and mid-term maintenance requirements into the economic model, assuming that stack replacement and maintenance expenditures occur during the project operation period. Since this work is primarily based on steady-state process simulation, a detailed dynamic degradation model was not further established. Instead, an equivalent life cycle discounting approach was adopted to account for maintenance and replacement costs in an aggregated manner. This treatment enables a more realistic representation of long-term operational economics while maintaining model simplicity.

The Total Capital Investment (TCI) comprises Fixed Capital Investment (FCI), Startup Costs (SC), and Working Capital (WC). FCI primarily includes Total Direct Costs (TDC) and Total Indirect Costs (TIC), both of which are calculated based on the Purchased Equipment Cost (PEC). TDC is further divided into Installed Direct Costs (IDC) and Non-Installed Direct Costs (NIDC).

In this study, Aspen Process Economic Analyzer (APEA) software is used to calculate the equipment costs for the green methanol synthesis system. Based on these costs, expenses related to installation, piping, electrical systems, civil engineering, engineering design, and other associated items are estimated with reference to literature data. Table 2 provides the definitions and calculation proportions for each component of TCI. Based on the actual Purchased Equipment Cost (PEC) of the project, Table 3 presents the detailed investment calculation results for the alkaline water electrolysis hydrogen production system. Together, these two tables form the complete basis for estimating the total project investment.

Table 2: Calculation of total project investment [17].

Item	Cost Calculation
Purchased Equipment Cost (PEC)	
Installed Direct Costs (IDC)	A + B + C + D + E
(A) Equipment Installation	39% PEC
(B) Instrumentation & Controls	26% PEC
(C) Piping	31% PEC
(D) Electrical Systems	10% PEC
(E) Service Facilities	55% PEC
Non-Installed Direct Costs (NIDC)	F + G + H
(F) Building & Construction	29% PEC
(G) Site Development	12% PEC
(H) Land	6% PEC
Total Direct Costs (TDC)	IDC + NIDC
Total Indirect Costs (TIC)	
(I) Engineering & Supervision	32% PEC
(J) Construction Overhead	34% PEC
(K) Contractors' Fees & Legal Expenses	23% PEC
(L) Contingency	37% PEC
Fixed Capital Investment (FCI)	TDC + TIC
Startup Costs (SC)	5% FCI
Working Capital (WC)	15% FCI
Total Capital Investment (TCI)	FCI + SC + WC

3.2.2 Operating Cost

Operating costs primarily consist of two components: Fixed Operation and Maintenance Costs (FOMC) and Variable Costs (VC). The fixed operation and maintenance costs are detailed in Table 3 below.

Table 3: Fixed operation and maintenance costs (FOMC) [18].

Item	Cost Calculation
Maintenance Labor	1.5% FCI
Maintenance Materials	1.5% FCI
Insurance & Taxes	1% FCI
Financing	10% WC
Labor (L)	9.4× h_{labor}
Supervision (S)	25% L
Direct Overhead (D)	50% (L + S)
General & Administrative	50% (L + S + D)
Total Fixed O&M Cost	FOMC

The Maintenance Materials cost is set at 1.5% of the Fixed Capital Investment (FCI) per year to cover scheduled component replacements over the 20-year project lifecycle. For the core alkaline electrolyzer, the electrode and diaphragm assemblies need replacement approximately every 10 years, which aligns with the 80,000-h stack durability benchmark under baseload conditions [16]. Additionally, since the proposed distributed hydrogen system integrates downstream fuel cells and buffer storage (as shown in Fig. 1), this 1.5% annualized factor also accounts for the long-term degradation of these auxiliary modules. Specifically, this 1.5% rate serves as a simplified annual average to cover both the main stack overhaul and the gradual performance decline of the auxiliary components, including the 0.5%/1000 h degradation rate for solid oxide fuel cell (SOFC) modules [19] and the 1.5–2% annual capacity fade for lithium-ion storage systems [20]. Using a flat annual percentage avoids complex yearly cost spikes while ensuring that the long-term replacement costs of these auxiliary modules are fully funded over the 20-year period. By correlating these literature-based degradation rates with the 1.5% FCI maintenance factor, the O&M cost estimation provides a realistic reflection of the lifecycle expenditures for the integrated distributed system.

Where h_{labor} represents the total labor hours, which can be derived from the empirical Eq. (19) [18]:

$$h_{\text{labour}} = 2.13 \times m_{\text{MeOH}}^{0.242} \times n_{\text{pro}} \times \frac{h_{\text{op}}}{24} \tag{19}$$

In the Equation, m_{MeOH} denotes the production capacity of the target product, n_{pro} denotes the number of process units, and h_{op} is the annual operating hours of the project, which is set as 8000 h in this study.

Variable costs (VC) primarily consist of the expenses incurred during the annual operation of the plant, including raw materials, electricity, water, utilities, catalysts, and other consumables. The variable costs for the green hydrogen production process are shown in the Table 4 below.

Table 4: Variable costs for green hydrogen production.

Variable Cost Item	Annual Consumption	Unit	Unit Cost (CNY)
KOH Replenishment	41.98	ton	9880.4/ton
Make-up Water	12.59	10^4 ton	20.4/ton
Electricity	800.68	GWh	0.32/kWh
Cooling Water	219.56	10^4 ton	0.0884/ton
Desiccant	12.59	ton	598.4/ton

The stochastic and intermittent nature of renewable energy sources (such as solar and wind) inherently leads to fluctuating and under-load operations of the distributed hydrogen production system. To account for this, the capacity factor is introduced as a macro variable in the techno-economic analysis. As noted by Glenk et al. [21] in their study on renewable power-to-gas economics, the instability of renewable power directly reduces equipment utilization, making the capacity factor a critical parameter for connecting these operational dynamics to the financial evaluation.

3.3 Energy and Exergy Analysis

The system's energy balance forms the foundation for evaluating the energy performance of the water electrolysis hydrogen production process. At its core is the adherence to the First Law of Thermodynamics, ensuring the conservation of energy entering and leaving the system. The general expression is:

$$\sum_{\text{in}} m_{\text{in}} h_{\text{in}} - \sum_{\text{out}} m_{\text{out}} h_{\text{out}} - W + Q = 0 \tag{20}$$

In the Equation, the four terms on the left side represent: the enthalpy of incoming streams, the enthalpy of outgoing streams, work done by the system (e.g., pump power consumption, typically negative), and heat exchange between the system and its surroundings.

To quantify the energy conversion efficiency of the electrolysis process, the energy efficiency of hydrogen production via water electrolysis, denoted as $\eta_{\text{en,H}_2}$, is defined. This efficiency reflects the ability to effectively convert input electrical energy (along with minor mechanical energy from auxiliary equipment) into the chemical energy of hydrogen fuel. Its calculation Equation is:

$$\eta_{\text{en,H}_2} = \frac{n_{\text{H}_2} \cdot \text{LHV}_{\text{H}_2}}{W_{\text{pump}} + W_{\text{elec}}} \tag{21}$$

In the Equation, the numerator n_{H2}·LHV_{H2} represents the thermal energy released by the complete combustion of the produced hydrogen (based on its lower heating value LHV), i.e., the effective chemical energy output of the hydrogen. The denominator $W_{\text{elec}} + W_{\text{pump}}$ denotes the total energy input driving the electrolysis process, including the electrical energy W_{elec} consumed by the electrolyzer and the mechanical energy W_{pump} consumed by auxiliary equipment such as circulation pumps within the system. This efficiency serves as a critical indicator for evaluating the technical and economic performance of the water electrolysis system, as its value directly influences the energy consumption level and operating costs of the hydrogen production process.

Exergy refers to the theoretical maximum amount of energy that can be converted into other forms when a system transitions from a specific state to equilibrium with environmental conditions. The environmental state is typically defined as a temperature of 25°C and a pressure of 1 atm. In steady-state industrial processes, the kinetic and potential energy terms are usually neglected. Exergy consists of physical exergy Ex_{ph} and chemical exergy Ex_{ch}, as expressed in Eq. (22):

$$Ex = Ex_{ph} + Ex_{ch} \tag{22}$$

Physical exergy can be calculated from the process state parameters of the system, as shown in Eq. (23):

$$Ex_{ch} = T_0(S_0 - S) - (H_0 - H) \tag{23}$$

where T_0, S_0 and H_0 represent the temperature, entropy, and enthalpy of the fluid under environmental conditions, respectively. S and H denote the entropy and enthalpy under working conditions. In this study, the physical exergy of each process system is calculated using Aspen Plus software. Chemical exergy can be determined based on the standard chemical exergy and the mole fractions of the fluid components. Specifically, the chemical exergy of a gas mixture can be calculated using Eq. (24):

$$Ex_{\text{ch, gas}} = RT_0 \sum x_i \ln x_i + \sum x_i Ex_{\text{ch0},i} \tag{24}$$

where x_i represents the mole fraction of each component, and $Ex_{\text{ch0},i}$ denotes the standard chemical exergy of each component at 25°C and 1 atm. The chemical exergy of non-gas mixtures can be expressed by Eq. (25) [22]:

$$Ex_{ch,\text{non-gas}} = \sum x_i Ex_{ch0,i} \tag{25}$$

The standard chemical exergies of each component are presented in Table 5.

Table 5: Standard chemical exergies of each component.

Component	Phase	Standard Chemical Exergy (kJ/mol)
Hydrogen (H_2)	Gas	236.09
Water (H_2O)	Gas	9.5
Water (H_2O)	Liquid	0.9
Oxygen (O_2)	Gas	3.97

The exergy balance calculation of the entire system can be expressed as Eq. (26):

$$Ex_{in,Q} + Ex_{\text{in},W} + m_{\text{in}} \sum Ex_{\text{in}} = Ex_{\text{out},Q} + Ex_{\text{out},W} + m_{\text{out}} \sum Ex_{\text{out}} + Ex_d \tag{26}$$

where Ex_{in} and Ex_{out} denote the exergies of the inlet and outlet fluids, respectively; Ex_Q and Ex_W represent the exergies associated with heat exchange, electricity, and work output of the system; and Ex_d is the exergy destruction. Ex_Q can be calculated by Eq. (27):

$$Ex_Q = Q\left(1 - \frac{T_0}{T}\right) \tag{27}$$

The exergy efficiency of the system can be obtained by Eq. (28):

$$\eta_{\text{ex},i} = \frac{Ex_{p,i}}{Ex_{m,Q} + Ex_{m,W} + m_m \sum Ex_m} \tag{28}$$

where $h_{\text{ex},i}$ refers to the exergy efficiency of each subsystem and the overall system, and $Ex_{p,i}$ represent the exergy value of the system products.

4 Results and Discussion

4.1 Life Cycle Assessment Results

The carbon emissions of hydrogen production via alkaline water electrolysis using renewable energy were analyzed through the life cycle carbon footprint analysis method. When photovoltaic energy was

adopted as the renewable energy, the life cycle carbon footprint of the hydrogen production process is presented in Fig. 3. The total carbon footprint of this production unit reached 1.94 kg CO_2eq/kg H_2.

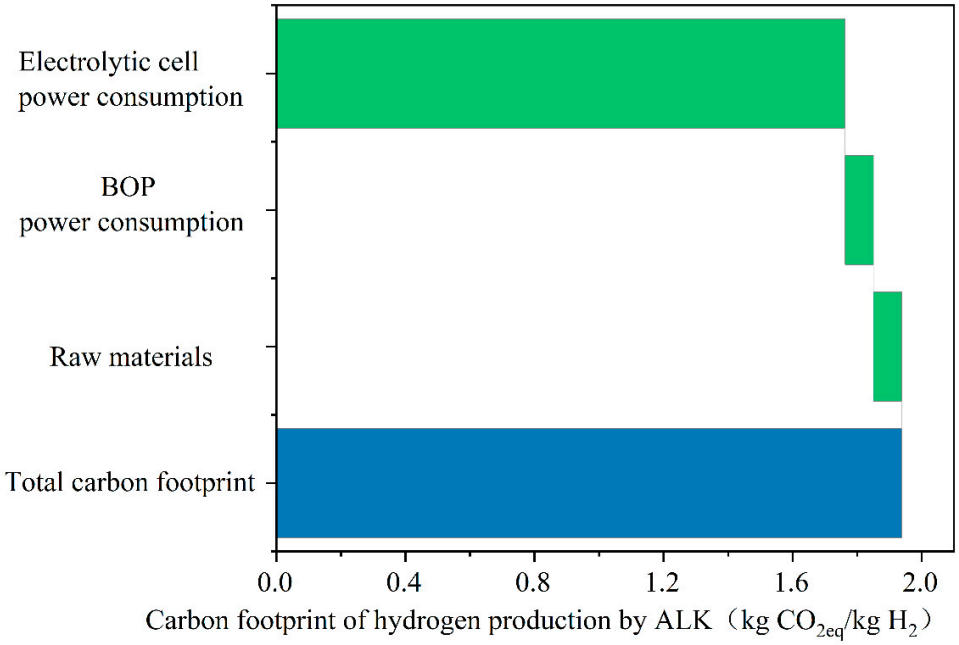


Figure 3: Life cycle carbon footprint analysis of hydrogen production via alkaline water electrolysis.

Specifically, the power consumption of the electrolyzer contributed approximately 1.76 kg CO_2eq/kg H_2 to the carbon footprint, accounting for 91% of the total, which highlights the critical role of energy utilization in this process. In contrast, the carbon emissions from the Balance of Plant (BOP) power consumption and raw materials exerted a relatively minor impact on the overall carbon footprint. The impacts of BOP power consumption and raw materials were both relatively small. These findings demonstrate that the power consumption of the electrolyzer constitutes the primary source of carbon emissions in this system. The results highlight the importance of improving energy efficiency and utilizing low-carbon electricity in the hydrogen production via water electrolysis.

When the carbon footprint of renewable energy fluctuates within the range of 0–100 kg CO_2eq/MWh, the variation in the total carbon footprint of hydrogen production via alkaline water electrolysis is presented in Fig. 4. The carbon footprints of renewable energy reported in different literatures and research institutions exhibit certain discrepancies. The abscissa corresponding to the color blocks in Fig. 4 represents the fluctuation range of carbon footprints for various renewable energy power generation technologies: hydropower is approximately 0–30 kg CO_2/MWh, wind power and nuclear power are roughly in the interval of 5–25 kg CO_2/MWh, while photovoltaic power generation is concentrated in a relatively high range of about 20–80 kg CO_2/MWh.

The height of the vertical color blocks indicates the possible variation range of the life cycle carbon emissions per unit of hydrogen, given a specific power carbon footprint interval and fixed electricity consumption for water electrolysis hydrogen production. In other words, it represents the envelope of the minimum and maximum values resulting from the combined effects of different system efficiencies, boundary conditions, and operating conditions.

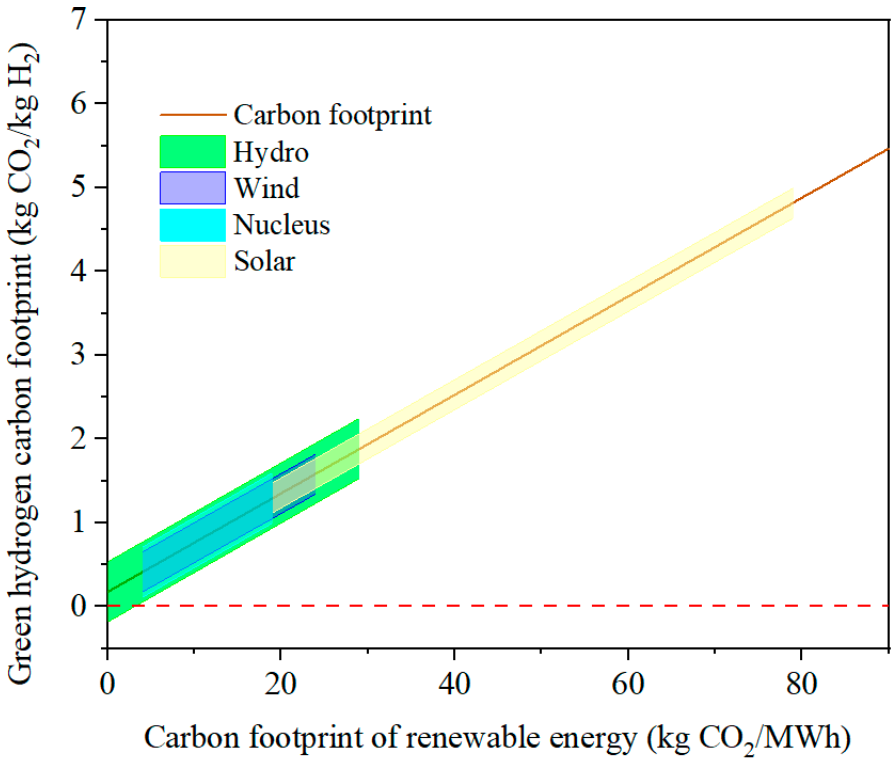


Figure 4: Comparative analysis of carbon footprints of water electrolysis hydrogen production driven by different renewable energy sources.

Additionally, to quantify the dynamic uncertainties embedded in the environmental metrics, the variance of the renewable power carbon intensity across different regions and source technologies (ranging from 0 to 100 kg CO_2eq/MWh) was systematically mapped out. This envelope analysis explicitly illustrates how upstream electricity emission factors propagate onto the total life cycle carbon footprint of green hydrogen, establishing the upper and lower feasibility boundaries under diverse regional power grids.

The results show that when hydropower is used as the renewable energy source, the carbon footprint of green hydrogen is the lowest, with a fluctuation range of 0.18–1.88 kg CO_2eq/kg H_2; when wind power is adopted, the fluctuation range of the green hydrogen carbon footprint is 0.41–1.59 kg CO_2eq/kg H_2. When nuclear power is utilized, the fluctuation range is 0.41–1.29 kg CO_2eq/kg H_2; and for photovoltaic power-driven hydrogen production, the fluctuation range is 1.29–4.82 kg CO_2eq/kg H_2. These results demonstrate that when renewable electricity is used-especially hydropower, wind power, and nuclear power-the life cycle carbon footprint per unit of hydrogen can be significantly lower than that of the traditional fossil fuel-based hydrogen production pathway. Although photovoltaic-driven hydrogen production has relatively higher carbon emissions, it can still achieve substantial emission reductions under reasonable equipment efficiency and power structure configurations.

4.2 Techno-Economic Assessment Results

In the total investment of a 100 MW-scale alkaline water electrolysis hydrogen production project, the equipment procurement cost amounts to 159.2 million CNY, which constitutes the core of the direct installation cost. With the specific breakdown presented in Table 6.

Table 6: Equipment procurement costs of alkaline water electrolysis hydrogen production project.

Process	Cost (10,000 CNY)
Electrolyzer Stacks	7164
Electrical System	4378
Deionized Water System	1926
Hydrogen Purification	1751
Gas Cooling	701
Total	15,920

For water electrolysis systems, the electrolyzer stack and auxiliary equipment may differ in terms of cost structure and installation characteristics. Therefore, the capital costs of the electrolyzer stack and other system components should be appropriately distinguished in techno-economic analysis. Reksten et al. developed a CAPEX model for PEM and alkaline water electrolysers, considering the effects of electrolyzer scale and technological development on capital costs [23]. Morgan et al. investigated the economies of scale of large-scale alkaline electrolyzers and evaluated the capital costs of major system components [24].

For the 100 MW alkaline water electrolysis system investigated in this study, the total purchased equipment cost is 159.20 million CNY, including 71.64 million CNY for the electrolyzer stacks and 87.56 million CNY for the remaining process equipment. Since the electrolyzer stack differs from conventional process equipment in terms of cost and installation characteristics, only 87.56 million CNY is used as the basis for calculating the conventional installation, non-installed direct, and indirect cost factors. In the subsequent preparation of the figure, the Purchased Equipment category retains the full equipment cost of 159.20 million CNY, including the electrolyzer stacks. Thus, the electrolyzer stack cost remains included in the project capital investment without being counted again through the conventional cost factors.

Based on the equipment procurement cost and incorporating the costs related to project construction, the total investment in the alkaline water electrolysis (AWE) system of this project reached 527.65 million CNY. The hierarchical breakdown of its capital cost is presented in Fig. 5. Of the total investment, the direct installation cost was 300.17 million CNY, with the equipment procurement cost accounting for 53.04%. The non-installation direct cost was 41.15 million CNY; the total indirect cost was 110.33 million CNY; and the other costs were 76.00 million CNY.

The annual operating cost of the project is 293.51 million CNY, with the breakdown shown in Fig. 6. The variable operating cost is the main component, accounting for 90.74% of the annual operating cost, within which the electricity cost for water electrolysis alone accounts for 96.20% of the variable cost. The fixed operation and maintenance (O&M) cost accounts for the remaining 9.26% of the total operating cost. This baseline cost structure establishes the deterministic economic foundation for the distributed alkaline water electrolysis (AWE) system prior to sensitivity analysis.

The variable cost calculation is based on the total capital investment and annual operating cost, with the capital recovery factor (CRF = 0.101852209) used for conversion. The levelized cost of hydrogen (LCOH) of the AWE system is calculated to be 25.40 CNY/kg, with its cost composition presented in Fig. 7. The annual operating cost accounts for 49.4% of the LCOH: among this, variable O&M cost accounts for 44.6% (of which electricity consumption constitutes the majority), and fixed O&M cost accounts for 4.9%. Capital expenditure accounts for 50.6%: with direct installation costs representing 25.3%, and the electrolyzer equipment procurement cost accounts for 57.5% of the direct installation cost, making it a key factor affecting the investment cost.

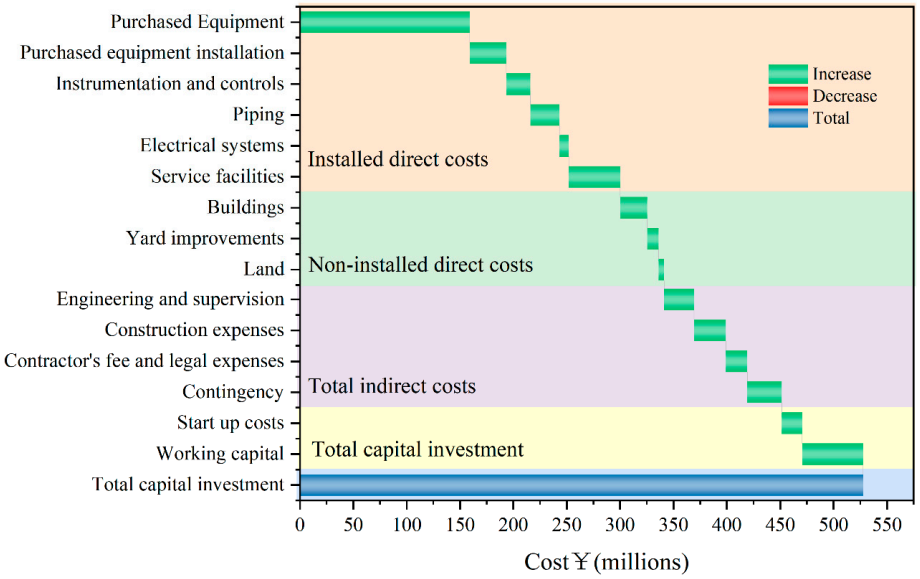


Figure 5: Investment cost of alkaline water electrolysis.

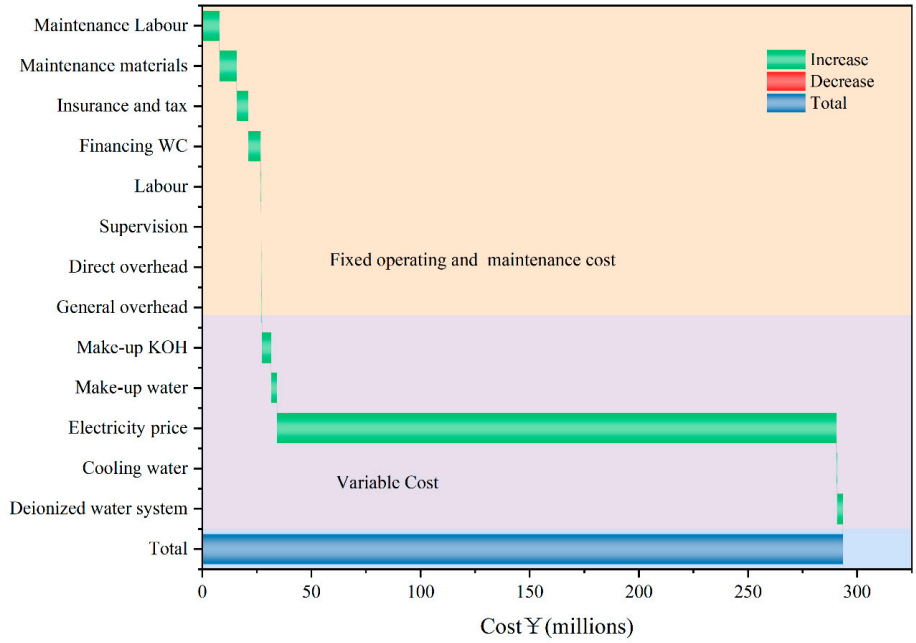


Figure 6: Operating cost breakdown of alkaline water electrolysis.

This cost structure clearly demonstrates that electricity costs are the primary driver of LCOH, while capital investment dominated by equipment procurement, also has a significant impact. These two factors jointly determine the economic boundary of the project. Compared to other mainstream hydrogen production technologies, the current cost of coal-to-hydrogen and natural gas steam methane reforming (SMR) hydrogen production in China is roughly in the range of 10–15 CNY/kg, and industrial by-product hydrogen is approximately 9–22 CNY/kg. Therefore, the cost in this study is still higher than that of traditional fossil energy-based hydrogen production and some by-product hydrogen pathways, and does not yet have a comprehensive advantage in terms of pure economics.

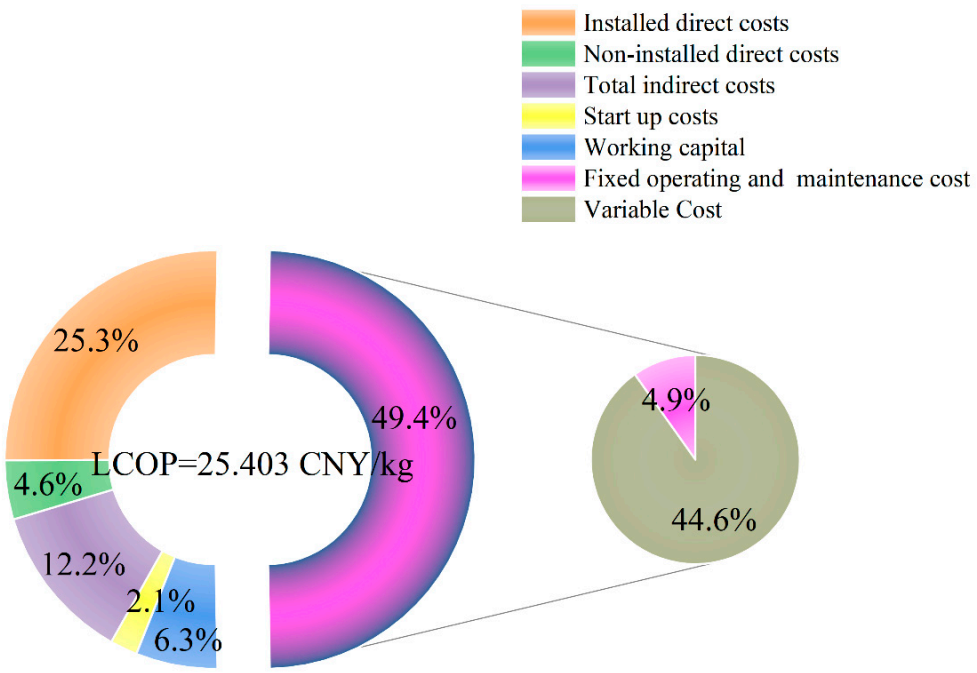


Figure 7: Levelized cost of hydrogen for alkaline water electrolysis hydrogen production projects.

However, when compared with other scenarios under the same water electrolysis technology route, the cost of alkaline water electrolysis hydrogen production is usually estimated to be around 30 CNY/kg when renewable electricity prices and equipment costs do not decrease significantly. The result of this study falls at the lower end of this range, indicating that, under reasonable renewable electricity prices and system parameters, distributed alkaline water electrolysis hydrogen production is expected to gradually narrow the cost gap with fossil-based hydrogen production, and lay a foundation for demonstrating its environmental advantages under future carbon constraints and carbon pricing scenarios.

As summarized in Table 7, the distributed alkaline water electrolysis hydrogen production system developed in this study exhibits competitive environmental performance compared with conventional fossil-fuel-based hydrogen production pathways. Coal-based hydrogen production and industrial by-product hydrogen generally maintain lower hydrogen production costs under current industrial conditions; however, these pathways are commonly associated with higher carbon emissions or limited resource availability. In contrast, the distributed AWE system investigated in this work achieves a life cycle carbon footprint of only 1.94 kg CO_2eq/kg H_2 under photovoltaic-powered conditions.

Furthermore, recent studies published between 2022 and 2024 indicate that the hydrogen production cost of centralized green hydrogen systems remains strongly dependent on renewable electricity prices, electrolyzer capital cost, and system utilization levels. PEM electrolysis systems generally exhibit superior dynamic response capability but are often associated with higher capital investment and system cost. Compared with these pathways, the distributed AWE system developed in this study demonstrates advantages in technological maturity, engineering applicability, and integrated environmental-economic performance under current industrial deployment conditions.

Based on these findings, the integration of dynamic time-of-use (TOU) electricity pricing and strategic off-peak power utilization (valley periods) emerges as a critical operational pathway to buffer the volatility of the LCOH. By shifting heavier water electrolysis loads to periods with surplus renewable generation or lower grid tariffs, the average electricity procurement cost can be effectively suppressed. This optimization

demonstrates that utilizing localized dynamic pricing mechanisms can drastically mitigate the negative economic impacts of renewable intermittency, thereby significantly enhancing the market competitiveness and financial robustness of distributed green hydrogen production units.

Table 7: Benchmark comparison of hydrogen production pathways reported in recent studies.

Roduction Pathway	Hydrogen Production Cost (CNY/kg)	Carbon Emission Characteristics	Technical Characteristics
Coal-based hydrogen production	7.24–10.13 CNY/kg [25]	High carbon emissions	Mature industrial technology
Industrial by-product hydrogen	9.12–11.65 CNY/kg [26]	Relatively high carbon emissions	Limited regional availability
Centralized green hydrogen systems	14–45 CNY/kg [27]	Low carbon emissions	Strong dependence on renewable electricity price and utilization level
PEM electrolysis systems	Generally higher than AWE systems [28]	Low carbon emissions	Fast dynamic response capability but relatively high capital cost
Distributed AWE system in this study	25.403 CNY/kg	1.94 kg CO_2eq/kg H_2	High technological maturity and suitable for distributed deployment

4.3 Energy and Exergy Analysis Results

The energy consumption of key components in the renewable energy hydrogen production system is presented in Fig. 8. In this system, the primary components of energy consumption are electricity and cooling energy. The total energy consumption is dominated by electricity, accounting for 97.5%. As the core component of the system, the electrolyzer (A101) is the major electricity-consuming unit.

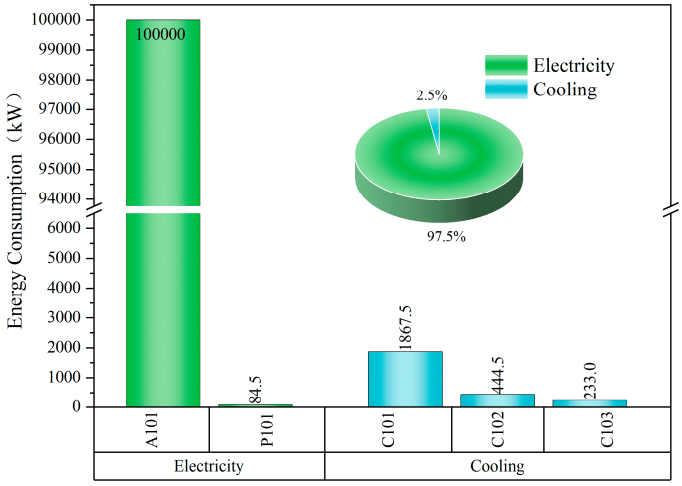


Figure 8: Energy consumption distribution of hydrogen production via water electrolysis.

In contrast, the energy consumption for cooling demand is relatively low, accounting for only 2.5% of the total energy consumption, and its distribution is relatively uniform. Specifically, the cooling demand of the cooler C101 is relatively high, reaching 1867.5 kW, followed by C102 and C103.

Overall, the electricity consumption is far higher than the cooling demand, which indicates that the main energy consumption of the system is concentrated in electricity usage. Accordingly, measures to reduce the electricity demand of A101 should be prioritized to improve energy utilization efficiency.

The exergy flow of the hydrogen production process via alkaline water electrolysis is presented in Fig. 9, which describes the exergy flow variation during the process in the form of a Sankey diagram. In the hydrogen production process via alkaline water electrolysis, the electrolyzer converts electrical energy into hydrogen energy, and exergy destruction within the electrolyzer accounts for the largest share.

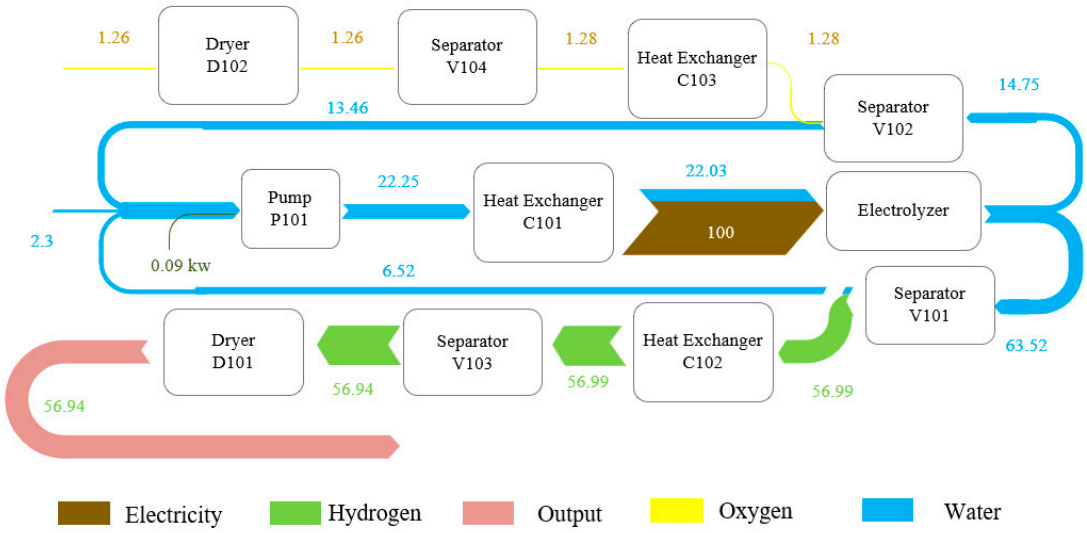


Figure 9: Exergy flow diagram of hydrogen production via alkaline water electrolysis.

With electrical energy input into the electrolyzer at a reference value of 100 MW, hydrogen and oxygen are output at different exergy flow rates after passing through various heat exchangers, separators and dryers. Among these streams, the exergy of the hydrogen stream decreases slightly when passing through equipment such as C102 and V101, while the water and recycle product streams circulate inside the system with minimal changes in stream values.

This indicates that the current process layout is relatively compact in terms of energy recovery and heat integration, with limited additional irreversible losses in auxiliary units. The key to further improving the second-law efficiency of the system lies in optimizing the electrolyzer design and operating conditions.

This Fig. 10 illustrates the process exergy destruction of each piece of equipment in the system. As can be seen from the exergy destruction diagram, the exergy destruction of the entire water electrolysis hydrogen production system is almost entirely concentrated in the electrolyzer itself. The exergy destruction of the electrolyzer (A101) is approximately 4.38×10^4 kW, accounting for 99.44% of the total exergy destruction, while the sum of exergy destruction of the cooling system, separators and pumps is less than 1%. Among this auxiliary equipment, the exergy destruction of the cooler C101 is about 220 kW, which is the highest proportion among auxiliary equipment but still negligible compared with that of the electrolyzer.

This indicates that the main source of system irreversibility lies in the electrode reactions and the heat and mass transfer processes inside the electrolyzer, whereas the processes such as heat exchange, separation and pumping have a weak impact on the overall efficiency. Therefore, to significantly reduce the total exergy destruction and improve the exergy efficiency of the system, the focus should be placed on optimizing the electrochemical reactions and heat and mass transfer processes inside the electrolyzer-such

as reducing overpotential, improving electrode and membrane materials, and enhancing the flow and heat transfer inside the electrolyzer.

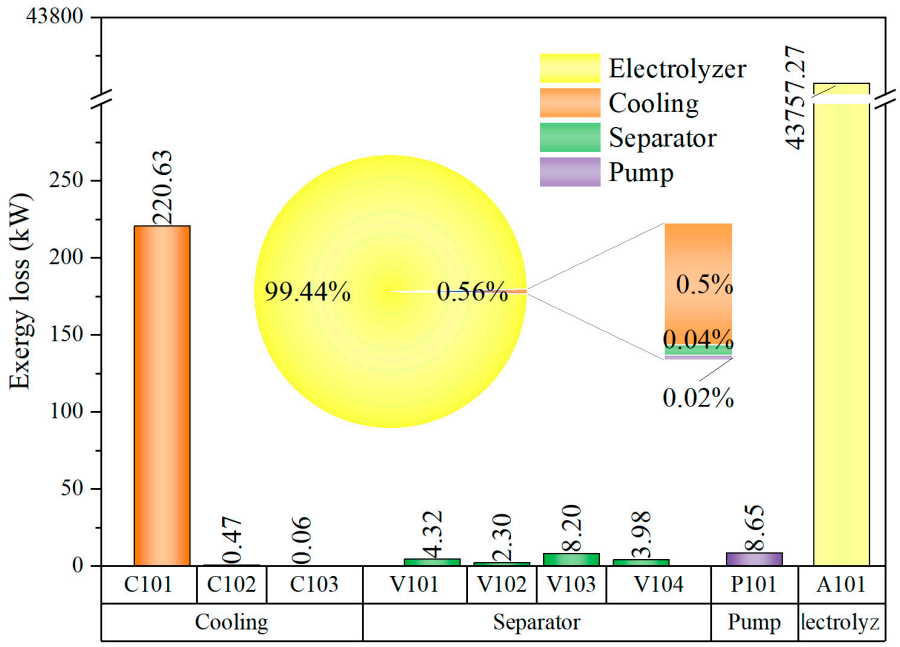


Figure 10: Distribution of exergy loss in water electrolyzer.

As can be seen from Table 8, the energy efficiency of hydrogen production via alkaline water electrolysis in this project is 56.57%, which is lower than the level of approximately 64.1% reported in the literature. This indicates that there is still room for optimization in terms of system integration, current density, or thermal management.

Table 8: Energy efficiency and exergy efficiency of hydrogen production via alkaline water electrolysis.

Index	This Project	Literature
Energy Efficiency	56.57%	64.1% [29]
Exergy Efficiency	55.61%	40.8%–59.4% [30]

The exergy efficiency of this project is 55.61%, which is slightly higher than the median value of the range of 40.8%–59.4% reported in the literature. This shows that after considering the energy grade, the effective utilization of input energy of this system is at the upper-middle level among existing studies.

Overall, the energy efficiency is slightly low while the exergy efficiency is relatively high. This suggests that subsequent efforts can focus on improving the energy efficiency by reducing the electrolyzer overpotential and the energy consumption of auxiliary equipment, while maintaining or further enhancing the exergy efficiency.

Sensitivity Analysis

To further investigate the variations in system economics driven by different technological advancement levels, and to systematically analyze the technical conditions and economic backgrounds required for the profitability of the distributed hydrogen production unit, a scenario-based financial evaluation was conducted based on three distinct techno-economic settings. The configurations for the three scenarios

are summarized in Table 9. Specifically, the system price of the water electrolysis unit fluctuates by ±50% around the baseline value of 1592 CNY/kW, defining the parameters for the "Bad" and "Good" scenarios, respectively. Based on the literature, the annual operating hours of the electrolyzer are set at 8000 h, 6000 h, and 4000 h for the Good, Basic, and Bad scenarios, respectively. The electrolyzer energy efficiency varies by ±10% from the baseline value of 56.6% to establish the boundaries for the Good and Bad scenarios. The selling prices of oxygen byproduct, renewable electricity, and ammonia across the three scenarios are determined according to current market conditions.

Table 9: Scenario parameters for the green electricity-powered hydrogen production unit.

Parameter	Good Scenario	Basic Scenario	Bad Scenario
Water electrolysis system price (CNY/kW)	796	1592	2388
Annual operating hours (h)	8000	6000	4000
Electrolyzer energy efficiency (%)	62.26	56.60	50.94
Oxygen price (CNY/t)	680	544	408
Renewable electricity price (CNY/kWh)	0.136	0.204	0.272

Under the three techno-economic backgrounds, the expected internal rate of return (ROR) is set at 4%, and the correspond ing Net Present Value (NPV) trajectories are illustrated in Fig. 11. Under the "Good" techno-economic scenario, the NPV crosses the zero-threshold in the third year, indicating that the project reaches the predefined return threshold within the third year and enters the profitable stage. Under the "Basic" scenario, the expected 4% ROR is approximately achieved at the end of the 20-year project lifespan. Conversely, under the "Bad" scenario, the NPV continuously declines, rendering the distributed hydrogen production unit economically unviable.

Utilizing the LCOH from the "Good" scenario as the baseline, the specific impacts on LCOH when each parameter varies between the Bad and Good boundaries are illustrated in Fig. 12. Among these variables, the electrolyzer energy efficiency and annual operating hours serve as the primary technical performance indicators, while the renewable electricity price, oxygen price, and water electrolysis system price constitute the key economic parameters. As indicated by the Tornado chart, the annual operating hours and renewable electricity price exhibit the most prominent impacts on the LCOH, serving as the dominant variables that govern the production cost of green hydrogen.

Transitioning from the worst-case condition (4000 h) to the best-case condition (8000 h) for the annual operating hours yields the largest variation band for the LCOH, spanning from approximately 32.00 CNY/kg down to 19.50 CNY/kg. This underscores that mitigating the negative economic impacts of renewable intermittency by maximizing the renewable utilization hours-and consequently extending the system's annual operating hours (serving as a macro proxy for the capacity factor)-represents a highly feasible and effective pathway to suppress the LCOH. Existing studies indicate that the annual utilization hours for onshore wind power typically range from 2800 h to 5100 h; solar photovoltaic generation ranges from 1000 h to 2200 h; while biomass power generation spans between 6000 h and 8300 h. Notably, integrating biomass power can reliably guarantee that the distributed green hydrogen production unit operates at a high-capacity factor and stable efficiency.

The renewable electricity price is similarly identified as a critical driver for the LCOH. When the electricity tariff drops from the worst-case (0.272 CNY/kWh) to the best-case (0.136 CNY/kWh) condition, the LCOH shifts from approximately 29.50 CNY/kg to 22.00 CNY/kg; on average, every 0.068 CNY/kWh reduction in the electricity price translates into a 3.75 CNY/kg decline in the LCOH.

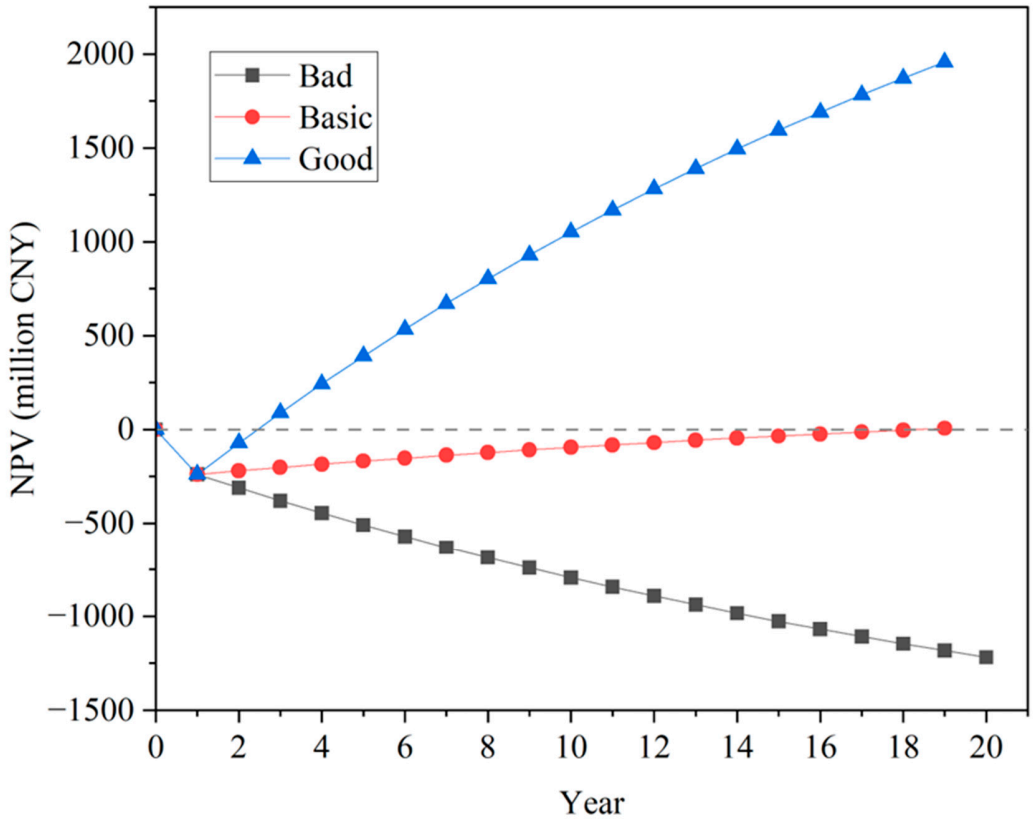


Figure 11: NPV variations of green hydrogen production under different scenarios.

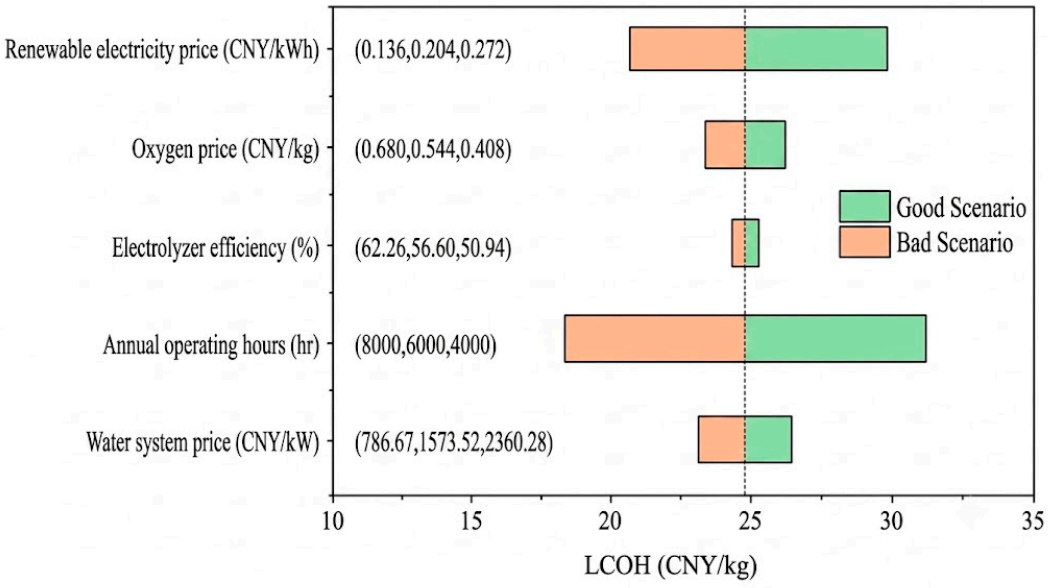


Figure 12: Scenario sensitivity analysis of levelized cost of green hydrogen production.

In contrast, the water electrolysis system price (ranging from 786.67 to 2360.28 CNY/kW), the oxygen byproduct price (ranging from 0.408 to 0.680 CNY/kg), and the electrolyzer energy efficiency (ranging from 50.94% to 62.26%) exert relatively limited impacts on the LCOH, displaying significantly narrower sensitivity bands. This indicates that, within the current techno-economic framework, prioritizing the reduction of

renewable power tariffs and maximizing the annual operating hours represent the most effective strategies to cutting down the LCOH of distributed green hydrogen.

The sensitivity analysis confirms that maximizing annual operating hours—serving as a macroscopic proxy for the capacity factor—is the most effective pathway to suppress the LCOH. However, relying on a flat capacity factor masks the physical friction of integrating intermittent renewables. A steady-state framework pro-vides a clean economic baseline, but a comprehensive evaluation must account for the dynamic operational realities of alkaline water electrolysis (AWE). Wind and solar power do not drop smoothly; they fluctuate wildly. This intermittency translates directly into two major operational challenges: partial-load efficiency drops and start-stop penalties.

This intermittency hits partial-load efficiency hard. As Buttler and Spliethoff [31] demonstrated, running an electrolyzer at low partial loads pushes the system into highly non-linear efficiency zones. The stack itself might see a slight thermodynamic efficiency bump at low currents because ohmic losses drop. But this small gain is quickly wiped out by the Balance of Plant (BoP). Heavy auxiliary systems—like electrolyte circulation pumps and thermal management units—have fixed base-load electricity demands. They cannot simply ramp down their draw to match the stack. Running at partial loads creates a massive parasitic energy drain, dragging down the system's actual energy efficiency far below steady-state assumptions.

Beyond efficiency losses, fluctuating power triggers severe start-stop penalties due to hard safety limits. When the renewable input drops the system below roughly 15–20% of its nominal load, the production volume of hydrogen and oxygen falls. The problem is that gas crossover through the diaphragm—which is driven by concentration gradients rather than the electrical current—stays roughly the same, as validated by Haug et al. [32]. This mismatch causes hydrogen to rapidly build up in the oxygen stream. Once that H_2-in-O_2 impurity approaches the critical 2 vol% safety limit, plant protocols force an immediate emergency shutdown to avoid explosion risks. In reality, intermittent renewable power doesn't just mean a lower capacity factor. It forces the electrolyzer into erratic, unscheduled start-stop cycles.

These repeated start-stop cycles take a severe physical toll over the project's lifetime. Sudden voltage shifts and thermal cycling cause the electrocatalysts to peel off and lose active surface area far faster than under stable conditions (Ursua et al. [13]). Steady-state frameworks assume a predictable, fixed stack lifespan. Dynamic operation shatters that assumption. From a life cycle assessment (LCA) perspective, faster degradation means replacing stacks more frequently, driving up the environmental footprint because manufacturing these components is highly energy-intensive. On the economic side (TEA), replacing stacks early inflates the reinvestment CAPEX. This pushes the true LCOH noticeably higher than what static models project. While the capacity factor remains a practical proxy for baseline economics, future system designs must integrate battery storage or advanced power electronics to buffer these real-world intermittency effects.

5 Conclusions

This study adopted a combined methodology of process simulation and life cycle assessment (LCA) to conduct a systematic analysis of the distributed alkaline water electrolysis (AWE) hydrogen production system driven by renewable energy, covering three dimensions: carbon footprint, economics, and energy utilization. A relatively comprehensive evaluation framework was thereby established. The key results are as follows:

(1) When renewable electricity is employed-particularly hydropower, wind power, and nuclear power-the life cycle carbon footprint per unit of hydrogen is significantly lower than that of traditional fossil fuel-based hydrogen production routes. Although photovoltaic (PV)-driven hydrogen production

exhibits slightly higher carbon emissions, it can still achieve substantial emission reductions under reasonable equipment efficiency and power structure configurations. Taking a typical PV scenario as an example, the total carbon footprint of the hydrogen production process is approximately 1.94 kg CO_2eq/kgH_2. Among this, electricity consumption by the electrolyzer contributes around 91%, while the contributions from balance of plant (BOP) power consumption and raw material emissions are minimal. This highlights the decisive role of electrolyzer energy efficiency and upstream electricity carbon intensity in determining the system's environmental performance.

(2) Economic analysis indicates that under the current technical level and cost assumptions, the levelized cost of hydrogen (LCOH) for distributed water electrolysis hydrogen production is 25.403 CNY/kg. Compared with other mainstream hydrogen production technologies, the cost in this study remains higher than that of traditional fossil energy-based hydrogen production and some by-product hydrogen routes, and thus does not yet possess a comprehensive advantage in terms of pure economics. However, with reasonable renewable electricity pricing and optimized system parameter settings in the future, distributed alkaline water electrolysis hydrogen production is expected to gradually narrow the cost gap with fossil-based hydrogen production, laying a foundation for demonstrating its environmental advantages under future carbon constraint and carbon pricing scenarios.

(3) Further energy and exergy analysis reveals that system irreversibility is highly concentrated in the electrolyzer itself, followed by a small number of heat exchange and cooling units, while exergy destruction in separation and pumping units is relatively limited. The overall energy efficiency and exergy efficiency are either comparable to or at the upper-middle level of values reported in the literature. Nevertheless, there remains room for improvement through measures such as reducing overpotential, optimizing internal flow fields, and enhancing heat integration.

Synthesizing the results from the environmental, economic, and energy perspectives, it can be concluded that distributed alkaline water electrolysis hydrogen production, when closely integrated with low-carbon electricity, holds significant emission reduction potential, making it a crucial technical pathway for decarbonizing end-use hydrogen consumption. Key factors influencing both the life cycle carbon footprint and hydrogen production cost include electrolyzer energy efficiency and renewable electricity carbon intensity. Furthermore, conducting exergy analysis at the system level is essential for accurately identifying where irreversible losses are concentrated, thus guiding equipment design and process optimization to improve overall system performance.

While the Aspen Plus framework provides a solid baseline for our exergy, economic, and environmental metrics, it remains a steady-state model. Relying on a flat capacity factor inevitably obscures the physical realities of renewable intermittency. For instance, this approach cannot capture the partial-load efficiency drops caused by BoP parasitic loads, nor does it reflect the accelerated stack degradation from frequent start-stop cycles. Moving forward, our next step is to address these modeling gaps. Future work will shift from deterministic scenarios to quantitative uncertainty analysis. By applying probabilistic tools like Monte Carlo simulations, we aim to define strict statistical confidence intervals for both the LCOH and the carbon footprint. Alongside this, we plan to expand the system boundaries to evaluate hybrid renewable configurations. Simulating solar-wind-storage architectures based on actual regional meteorological data will allow us to investigate how short-term energy storage can buffer transient fluctuations. This coordinated modeling approach is essential to mitigate the dynamic penalties identified in the current study and fully optimize distributed green hydrogen systems.

Acknowledgement: We are very grateful for the support of State Grid Jiangsu Electric Power Company.

Funding Statement: The study was supported by the Science and Technology Projects of State Grid Jiangsu Electric Power Company "Research on Site Selection Planning and Capacity Configuration Optimization of Distributed Hydrogen Production Stations in Transformer Areas Oriented to Distribution Network Interaction, JCCZ2025002".

Author Contributions: Study conception and design: Yutong Lei; data collection: Zhongchao Yang; analysis and interpretation of results: Xingyu Liu; draft manuscript preparation: Mingtao Tang; draft manuscript preparation: Mingchen Yao. All authors reviewed and approved the final version of the manuscript.

Availability of Data and Materials: Due to the nature of this research, participants of this study did not agree for their data to be shared publicly, so supporting data is not available.

Ethics Approval: Not applicable.

Conflicts of Interest: The authors declare no conflicts of interest.

References

1. Ozcan H, El-Emam RS, Celik S, Amini Horri B. Recent advances, challenges, and prospects of electrochemical water-splitting technologies for net-zero transition. Clean Chem Eng. 2023;8:100115. [CrossRef].
2. Jang D, Kim J, Kim D, Han WB, Kang S. Techno-economic analysis and Monte Carlo simulation of green hydrogen production technology through various water electrolysis technologies. Energy Convers Manag. 2022;258:115499. [CrossRef].
3. Sebbahi S, Nabil N, Alaoui-Belghiti A, Laasri S, Rachidi S, Hajjaji A. Assessment of the three most developed water electrolysis technologies: alkaline water electrolysis, proton exchange membrane and solid-oxide electrolysis. Mater Today Proc. 2022;66:140–5. [CrossRef].
4. Öhman A, Karakaya E, Urban F. Enabling the transition to a fossil-free steel sector: the conditions for technology transfer for hydrogen-based steelmaking in Europe. Energy Res Soc Sci. 2022;84:102384. [CrossRef].
5. Chehade Z, Mansilla C, Lucchese P, Hilliard S, Proost J. Review and analysis of demonstration projects on power-to-X pathways in the world. Int J Hydrogen Energy. 2019;44(51):27637–55. [CrossRef].
6. Mulder FM, Weninger BMH, Middelkoop J, Ooms FGB, Schreuders H. Efficient electricity storage with a battolyser, an integrated Ni–Fe battery and electrolyser. Energy Environ Sci. 2017;10(3):756–64. [CrossRef].
7. Kumar SS, Lim H. An overview of water electrolysis technologies for green hydrogen production. Energy Rep. 2022;8:13793–813. [CrossRef].
8. Zhang WQ, Yu B. Development status and prospects of high-temperature solid oxide electrolysis for hydrogen production. J Electrochem. 2020;26(2):212–29. (In Chinese). [CrossRef].
9. Boardman RD. Figures of merit for nuclear/hydrogen hybrid systems. Idaho Falls, ID, USA: Idaho National Laboratory; 2017.
10. Terlouw T, Bauer C, McKenna R, Mazzotti M. Large-scale hydrogen production via water electrolysis: a techno-economic and environmental assessment. Energy Environ Sci. 2022;15(9):3583–602. [CrossRef].
11. Ajeeb W, Costa Neto R, Baptista P. Life cycle assessment of green hydrogen production through electrolysis: a literature review. Sustain Energy Technol Assess. 2024;69:103923. [CrossRef].
12. Lee B, Cho HS, Kim H, Lim D, Cho W, Kim CH, et al. Integrative techno-economic and environmental assessment for green H_2 production by alkaline water electrolysis based on experimental data. J Environ Chem Eng. 2021;9(6):106349. [CrossRef].
13. Ursua A, Gandia LM, Sanchis P. Hydrogen production from water electrolysis: current status and future trends. Proc IEEE. 2012;100(2):410–26. [CrossRef].
14. Sundha P, Melkania U. Carbon footprinting: a tool for environmental management. Int J Agric Environ Biotechnol. 2016;9(2):247. [CrossRef].
15. Fang K, Heijungs R, de Snoo GR. Theoretical exploration for the combination of the ecological, energy, carbon, and water footprints: overview of a footprint family. Ecol Indic. 2014;36:508–18. [CrossRef].
16. IEA. Electrolysers, IEA Energy System Report [Internet]. 2024 [cited 2026 Sep 16]. Available from: https://www.iea.org/energy-system/low-emissions-fuels/electrolysers.

17. Dimitriou I, Goldingay H, Bridgwater AV. Techno-economic and uncertainty analysis of Biomass to Liquid (BTL) systems for transport fuel production. Renew Sustain Energy Rev. 2018;88:160–75. [CrossRef].
18. Fernanda Rojas Michaga M, Michailos S, Akram M, Cardozo E, Hughes KJ, Ingham D, et al. Bioenergy with carbon capture and storage (BECCS) potential in jet fuel production from forestry residues: a combined Techno-Economic and Life Cycle Assessment approach. Energy Convers Manag. 2022;255:115346. [CrossRef].
19. Zarabi Golkhatmi S, Asghar MI, Lund PD. A review on solid oxide fuel cell durability: latest progress, mechanisms, and study tools. Renew Sustain Energy Rev. 2022;161:112339. [CrossRef].
20. Grimaldi A, Minuto FD, Perol A, Casagrande S, Lanzini A. Techno-economic optimization of utility-scale battery storage integration with a wind farm for wholesale energy arbitrage considering wind curtailment and battery degradation. J Energy Storage. 2025;112:115500. [CrossRef].
21. Glenk G, Reichelstein S. Economics of converting renewable power to hydrogen. Nat Energy. 2019;4(3):216–22. [CrossRef].
22. Li G, Liu Z, Liu F, Yang B, Ma S, Weng Y, et al. Advanced exergy analysis of ash agglomerating fluidized bed gasification. Energy Convers Manag. 2019;199:111952. [CrossRef].
23. Reksten AH, Thomassen MS, Møller-Holst S, Sundseth K. Projecting the future cost of PEM and alkaline water electrolysers; a CAPEX model including electrolyser plant size and technology development. Int J Hydrogen Energy. 2022;47(90):38106–13. [CrossRef].
24. Morgan ER, Manwell JF, McGowan JG. Opportunities for economies of scale with alkaline electrolyzers. Int J Hydrogen Energy. 2013;38(36):15903–9. [CrossRef].
25. Fan JL, Yu P, Li K, Xu M, Zhang X. A levelized cost of hydrogen (LCOH) comparison of coal-to-hydrogen with CCS and water electrolysis powered by renewable energy in China. Energy. 2022;242:123003. [CrossRef].
26. Zhang X, Qian X, Xiao C, Yin X, Wang X, Wang Z, et al. Advancements in purification and holistic utilization of industrial by-product hydrogen: progress, challenges, and prospects. Green Energy Resour. 2024;2(4):100098. [CrossRef].
27. Gómez J, Castro R. Green hydrogen energy systems: a review on their contribution to a renewable energy system. Energies. 2024;17(13):3110. [CrossRef].
28. Abdelsalam RA, Mohamed M, Farag HEZ, El-Saadany EF. Green hydrogen production plants: a techno-economic review. Energy Convers Manag. 2024;319:118907. [CrossRef].
29. Ding S, Guo B, Hu S, Tian Z, Gu J, Zhang T, et al. Experimental and modeling study on energy flow of 250 kW alkaline water electrolysis system under steady state conditions and cold start process. Fuel. 2023;350:128799. [CrossRef].
30. Ding S, Guo B, Hu S, Gu J, Yang F, Li Y, et al. Analysis of the effect of characteristic parameters and operating conditions on exergy efficiency of alkaline water electrolyzer. J Power Sources. 2022;537:231532. [CrossRef].
31. Buttler A, Spliethoff H. Current status of water electrolysis for energy storage, grid balancing and sector coupling via power-to-gas and power-to-liquids: a review. Renew Sustain Energy Rev. 2018;82:2440–54. [CrossRef].
32. Haug P, Koj M, Turek T. Influence of process conditions on gas purity in alkaline water electrolysis. Int J Hydrogen Energy. 2017;42(15):9406–18. [CrossRef].